Environ. Process. (2015) 2:773–796
DOI 10.1007/s40710-015-0117-z

ORIGINAL ARTICLE

Adsorption of Phenol from Aqueous Solution Using *Lantana camara*, Forest Waste: Packed Bed Studies and Prediction of Breakthrough Curves

C. R. Girish[1] · **V. Ramachandra Murty**[2]

Received: 1 April 2015 / Accepted: 12 October 2015 / Published online: 28 October 2015

Abstract In this paper, the feasibility of the dry stem of *Lantana camara* waste as an adsorbent to remove phenol from aqueous solution was investigated in a packed-bed column. The effect of bed height (5, 10, 15 cm), initial phenol concentration (100, 150, 250 mg L^{-1}) and feed flow rate (10, 15, 20 mL min^{-1}) on the adsorption were studied by evaluating the breakthrough curves. The following models were used to assess the column performance: Thomas, Adams-Bohart, Yoon Nelson, Modified dose–response, linear driving force model based on fluid phase concentration difference (LDFC) and linear driving force model based on particle phase concentration difference (LDFQ). The Thomas model and the LDFC model were in good agreement with the experimental data. The bed depth service time (BDST) model was used to predict adsorption performance at other experimental conditions. The maximum adsorption capacity was found to be 149.77 mg g^{-1}, confirming that *Lantana camara* is a suitable adsorbent for the removal of phenol from aqueous solution.

Keywords Adsorption · Forest waste · Packed bed column · Breakthrough curves

1 Introduction

The wastewater released from the chemical industries contains various pollutants like phenol, dyes, organic matter, heavy metals and suspended matter (Reza Rahmani et al. 2015). Among them, phenol is one of the crucial pollutants present in wastewater released at noticeable levels. The concentrations of phenol in wastewater released from various industries are listed in Table 1 (Polat et al. 2006; Ucun et al. 2010). The inclusion of a wastewater management and pollution control target is, therefore, an essential component of any future water agenda (Karnib 2014).

✉ C. R. Girish
girishcr1@rediffmail.com

[1] Department of Chemical Engineering, MIT, Manipal 576104 Karnataka, India

[2] Department of Biotechnology, MIT, Manipal 576104 Karnataka, India

Table 1 The concentration of phenol in wastewater released from various industries

Industrial source	Phenol concentration, mg L^{-1}
Petroleum refineries	40–185
Petrochemical	200–1220
Textile	100–150
Leather	4.4–5.5
Coke ovens	600–3900
Coal conversion	1700–7000
Ferrous industry	5.6–9.1
Rubber industry	3–10
Pulp and paper industry	22
Wood preserving industry	50–953
Phenolic resin production	1600
Phenolic resin	1270–1345
Fiberglass manufacturing	40–2564
Paint manufacturing	1.1

Various treatment methods, such as biodegradation, biosorption, membrane separation, pervaporation, solvent extraction, distillation and adsorption using activated carbon prepared from various precursors are available to remove phenolic compounds from aqueous solution.

Adsorption on activated carbon is one of the efficient methods in treating wastewater. Activated carbon can be formed from any carbonaceous precursor material. A vast number of materials have also been examined as potential adsorbents for phenol removal in wastewater treatment. The eminent among them includes silica gel (Førland and Blokhus 2007; An et al. 2009), red mud (Wang et al. 2008; Tor et al. 2006), zeolites (Damjanović et al. 2010; Yousef and El-Eswed 2009; Melidis 2015), activated alumina (Danis et al. 1998; Adak and Pal 2006) and activated carbon. But because of the expensive nature of the above materials, there is a need to do further research to produce adsorbents from locally available agricultural materials (Hartmann et al. 2014; Banat and Al-Asheh 2000).

Earlier research on adsorption were limited to batch studies. This may be because of the limitation due to the unavailability of large quantity of adsorbent material (Vijayaraghavan et al. 2004). Batch adsorption processes may not be a suitable method at the industrial scale to deal with high flow rates (Karunarathne and Amarasinghe 2013). However, such experiments are conducted to measure the effectiveness of process in removing specific adsorbates and to find the maximum adsorption capacity (Ahmad and Hameed 2010). The working principle of batch studies is that the same feed solution remains in contact with the adsorbent. The process continues till equilibrium is established between the adsorbate and the adsorbent. After the equilibrium is established, the same solution remains in the system. Therefore, the efficiency of the process decreases, the adsorbent may not be utilized effectively, the volume of the effluent treated decreases and the adsorption capacity decreases (Dwivedi et al. 2008).

Therefore, in order to overcome all these difficulties, continuous mode of experiments is advised over batch studies. The various continuous mode studies available are: packed bed, fluidised bed, inverse fluidised bed, and trickle bed columns. The mechanism of packed column is that the feed solution flows continuously inside the column and the adsorbent will be in continuous contact with the feed solution. In such mode of operations, all the active sites

on the adsorbent will be occupied and the adsorbent will be used up completely. Thus, a packed bed column offers a vast number of advantages of operational simplicity, handling large influent flow rates, obtaining high yields and scaling up of the processes (Vázquez et al. 2006). The packed column also makes best use of the concentration difference as the driving force required for adsorption which results in a better quality of the effluent (Aksu and Gönen 2004). The packed columns can also be utilized for treating wastewater containing various pollutants released from various industries (Tepe and Dursun 2008). The performance of these columns are measured by evaluating the variation in concentrations with respect to time which leads to the generation of breakthrough curves. The various packed bed models available in the literature are useful in understanding the adsorption processes which are also crucial in deciding the process parameters (Zhang et al. 2011).

A large number of agricultural waste materials have been used as adsorbents for the removal of various pollutants from wastewater, including phenol, in packed bed studies. The prominent among them are olive pomace (Banat et al. 2007), jackfruit peel (Tamez Uddin et al. 2009), phoenix leaf powder (Han et al. 2009), corn stalk (Chen et al. 2012), *Agaricus bisporous* (Long et al. 2014), biomass (Mishra et al. 2013), chitosan (Auta and Hameed 2014), cassava peel (Simate and Ndlovu 2015), *Prosopis juliflora* (Gopal et al. 2014). All these materials provide a substitute to conventional sources, which can be prospective raw materials for activated carbon production. Therefore, in the search for new agricultural wastes as precursor for adsorbents, efforts have been made to produce adsorbents from dry bark of lantana trees by chemical treatment process (Girish and Ramachandra Murty 2014).

Lantana camara is an invasive poisonous forest weed, abundantly found in all parts of the world (Priyanka and Joshi 2013). It changes fire regimes resulting in major threats to ecosystem. In the current work, lantana barks were collected from tropical moist deciduous forests, i.e., eastern side of western ghats in Coorg region, Karnataka, India. In previous studies, the potential of chemically treated carbon from lantana dry bark were studied in batch mode for the removal of phenol from aqueous solution. The adsorption of phenol on adsorbent treated with HCl or KOH has also been reported in previous work (Girish and Ramachandra Murty 2014). The conclusion was that *Lantana camara* treated with HCl or KOH can achieve adsorption capacity of 112.5 and 91.07 mg g^{-1}, respectively (Girish and Ramachandra Murty 2014).

In order to improve the adsorption capacity aiming at industrial applications, column studies were undertaken. In this study, a systematic column investigation of the phenol adsorption on chemically treated lantana barks was reported to improve the efficiency of the process. The study tested the effect of different operating parameters on adsorption, such as variation of flow rate, initial concentration of phenol and bed length. The prediction of the breakthrough curves and the validation to different packed bed models like Thomas, Adams-Bohart, Modified dose-response, Clark, Yoon-Nelson, LDFC and LDFQ models were done which shows the behaviour of the adsorption processes. This study also used the BDST model which is essential in designing the process parameters.

2 Theoretical Investigation

2.1 Adsorption Parameter Estimation

The various process parameters such as the quantity adsorbed at breakthrough time and at saturation time, removal percentage of phenol, the effluent volume, uptake capacity, fractional

bed utilization, mass transfer zone and the slope of the breakthrough curve were investigated to evaluate the column performance. The above parameters will provide the information on the column performance which will be useful in the design of the column.

The breakthrough curves are drawn by plotting the relative concentration of phenol, which is the ratio of the phenol concentration in the effluent to the concentration in the feed solution with respect to time. The total phenol adsorbed (q_{total}) is determined from the area under the curve of adsorbed phenol concentration (C_{ad}) versus time (t) multiplied by the flow rate, according to the following equation (Aksu and Gönen 2004):

$$q_{total} = \frac{F}{1000} \int_{t=0}^{t=t_{total}} C_{ad}\, dt \tag{1}$$

where F is the flow rate (mL min^{-1}); t_{total} is the total flow time (min); C_{ad} is the adsorbed concentration (mgL^{-1}).

The maximum adsorption capacity (q_{eq}) can be calculated from the Eq. (2) (Aksu and Gönen 2004):

$$q_{eq} = \frac{q_{total}}{m} \tag{2}$$

where m is the amount of the adsorbent (g).

The quantity of phenol sent to the column (m_{total}) is given in Eq. (3) (Han et al. 2009):

$$m_{total} = \frac{C_0 F t_{total}}{1000} \tag{3}$$

where C_0 is the initial phenol concentration (mg L^{-1}).

The total phenol removed (*% rem*) with respect to the phenol feed entering the column is given by Eq. (4):

$$\%rem = \frac{q_{total}}{m_{total}} \times 100 \tag{4}$$

Effluent volume (*Veff*) is calculated from the Eq. (5) (Volesky et al. 2003):

$$V_{eff} = F t_{total} \tag{5}$$

where t_{total} is the total flow time (min).

The adsorption uptake (q_b) at breakthrough time (t_b) is obtained by Eq.(6) (Long et al. 2014):

$$q_b = \frac{C_0 F}{w} \int_0^{t_b} C_{ad}\, dt \tag{6}$$

where t_b is the time needed for the outlet concentration to reach 10 % of initial concentration (min).

Similarly the adsorption uptake (q_s) at saturation time (t_s) is obtained as (Long et al. 2014; Sotelo et al. 2013a):

$$q_s = \frac{C_0 F}{w} \int_0^{t_s} C_{ad}\, dt \tag{7}$$

where t_s is the desired time (min) for the outlet concentration to reach 90 % of initial concentration.

The mass transfer zone (MTZ) is calculated from Eq. (8). (Sotelo et al. 2013a, b; Nuić et al. 2013):

$$\mathrm{MTZ} = \mathrm{Z} \times \left(1 - \frac{\mathrm{t_b}}{\mathrm{t_s}}\right) \tag{8}$$

where Z is the length of the bed (cm).

The Fractional bed utilization (*FBU*) parameter shows the fraction of packed column used for the adsorption process. It is given by Eq. (9) (Sotelo et al. 2013a, b):

$$\mathrm{FBU} = \frac{\mathrm{q_b}}{\mathrm{q_s}} \tag{9}$$

The slope of the breakthrough curve (dc/dt) which shows the nature of the breakthrough curve between 10 and 90 % saturation of the bed was also calculated.

2.2 Modelling the Column Data

Many models have been developed for illustrating the column behaviour and performance. The prediction of breakthrough curve and the estimation of the maximum adsorption capacity is important in the design of an adsorption column.

2.2.1 Thomas Model

The model assumes plug flow behaviour, employs Langmuir isotherm for equilibrium, and second-order reversible reaction kinetics. This model is generally used for adsorption processes where the external and internal diffusion limitations are absent. The model also explains that the inter-phase mass transfer is the rate limiting step (Mitra et al. 2014; Ahmad and Hameed 2010; Su et al. 2013). It also describes that the process can be applied to systems which follows either favorable or unfavorable isotherms (Song et al. 2011). The linear form of the Thomas model is given by :

$$\ln\left(\frac{\mathrm{C_t}}{\mathrm{C_o}} - 1\right) = \left(\frac{\mathrm{k_{Th}} \mathrm{q_{eq}} \mathrm{m}}{\mathrm{F}} - \mathrm{k_{Th}} \mathrm{C_o} \mathrm{t}\right) \tag{10}$$

where C_o and C_t are the inlet and outlet phenol concentrations (mg L^{-1}); k_{Th} is the Thomas rate constant (mL min^{-1} mg^{-1}); q_{eq} is the theoretical equilibrium phenol uptake per gram of the adsorbent (mg g^{-1}); m is the amount of the adsorbent in the column (g); and F is the flow rate of the solution through the column (mL min^{-1}). The constants k_{Th} and q_{eq} can be calculated from the linear plot of $ln\left(\frac{C_t}{C_o} - 1\right)$ versus t.

2.2.2 Adams-Bohart Model

The model is used in describing the initial part of the breakthrough curve (Ahmad and Hameed 2010; Mitra et al. 2014). The model explains that the kinetics was controlled by external mass transfer in the initial part of adsorption (Chen et al. 2012). This model is also based on the postulate that the adsorption rate is proportional to the

residual capacity of adsorbent and the solute concentration (Aksu and Gönen 2004; Saad et al. 2014; Dutta and Basu 2014). The expression for the model is given by

$$\ln\left(\frac{C_t}{C_o}\right) = k_{AB}C_o t - \frac{k_{AB}N_o z}{v} \tag{11}$$

where C_o and C_t are the inlet and outlet concentration of phenol (mg L^{-1}); k_{AB} is the kinetic constant (L mg^{-1} min^{-1}); v is the linear velocity (cm min^{-1}); Z is the length of the bed (cm) and No is the saturation concentration (mg L^{-1}). The values of k_{AB} and No were determined from the slope and intercept of the linear plot of $\ln(C_t/C_o)$ against time t.

2.2.3 Yoon- Nelson Model

The Yoon-Nelson model was derived based on the assumption that the rate of decrease in the probability of adsorption of adsorbate molecule is proportional to the probability of the adsorbate adsorption and the adsorbate breakthrough on the adsorbent (Yoon and Nelson 1984; Saad et al. 2014; Dutta and Basu 2014). The linearized form of the model is represented as:

$$\ln\left(\frac{C_t}{C_t - C_o}\right) = k_{YN}t - k_{YN}\tau \tag{12}$$

where k_{YN} is the rate constant (min^{-1}); τ is the time required for 50 % adsorbate breakthrough (min). The constants k_{YN} and τ can be determined from the slope and intercept of the linear plot of $\ln[C_t/(C_o - C_t)]$ against time t.

2.2.4 Modified Dose–Response Model

The Modified dose–response model reduces the errors that arise from use of the Thomas model, particularly in the initial and final part of breakthrough curve (Song et al. 2011; Gokhale et al. 2009; Su et al. 2013). The linear model has the following form:

$$\ln\left(\frac{C_o}{C_t} - 1\right) = a \times \ln b - a \times \ln(F \times t) \tag{13}$$

Parameters a and b can be calculated from the model. The parameter q_{eq} is the theoretical adsorption capacity (mg g^{-1}); m is the mass of the adsorbent in the column (g); and F is the flow rate of the solution through the column (mL min^{-1}). From the value of b, the value of adsorption capacity q_{eq} can be calculated using the expression:

$$q_{eq} = \frac{b\, C_o}{m} \tag{14}$$

2.2.5 LDFC Model

The LDFC model is applied when the fluid phase concentration difference is the driving force for adsorption process. It is also based on the fact that mass transfer

from the fluid phase to the solid surface dominates the process. The expression is as follows (Lua and Jia 2009)

$$t = t_o + \frac{\rho_b q_o / C_o}{k_f}\left(1 - \frac{R\ln(1-x) - \ln x}{1-R}\right) \tag{15}$$

where t_o is the characteristic time (min); ρ_b is the bulk density of bed (g cm^{-3}); q_o is the solid phase concentration in equilibrium with C_o, (mg g^{-1}); C_o is the initial phenol concentration (mg L^{-1}); k_f is the fluid-to-particle mass transfer coefficient (min^{-1}); R is the equilibrium parameter for adsorption; x is the dimensionless outlet concentration ($x = C_t/C_o$). The characteristic time (t_o) and the mass transfer coefficient (k_f) can be calculated from the intercept and slope of the plot of 1-((Rln(1-x)-lnx)/(1-R) against t. The value of equilibrium parameter (R) can be taken from the batch studies and is given by expression

$$R = \frac{1}{(1 + bC_o)} \tag{16}$$

where b is the Langmuir constant (Lmg^{-1})

2.2.6 LDFQ Model

The LDFQ model is used when the particle phase concentration difference is the driving force for adsorption (Lua and Jia 2009; Zhang et al. 2011). The model is developed on the probable reason that intraparticle diffusion is the rate-limiting step. The model is represented as

$$t = t_o + \frac{\rho_b}{k_s}\left(\frac{R}{1-R}\ln x - \frac{1}{1-R}\ln(1-x) - 1\right) \tag{17}$$

where t_o is the characteristic time (min); ρ_b is the bulk density of bed (g cm^{-3}); k_s is the fluid-to-particle mass transfer coefficient (min^{-1}); R is the equilibrium parameter from batch studies; x is the dimensionless outlet concentration ($x = C_t/C_o$). The characteristic time (t_o) and the mass transfer coefficient can be calculated from the intercept and slope of the plot of $(\frac{R}{1-R} ln x - \frac{1}{1-R} ln\ (1-x)\ -1)$ v/st.

The various models used for evaluating the adsorber performance, its linear form and the mathematical form for finding the breakthough curve are summarized in Table 2.

2.3 Design of Adsorption Column

BDST model describes the linear relationship between bed depth, Z, and service time, t, in terms of process parameters like initial phenol concentration, flow rate and the adsorption capacity. The service time is defined as the time up to which the adsorbent will be able to remove the pollutant from the wastewater before regeneration is needed (Markovska et al. 2001). It also shows the time taken by the column to reach the breakthrough point (Han et al. 2009). The model is based on the assumption that the rate of adsorption is limited by the surface reaction between adsorbate and the unused capacity of the adsorbent (Goel et al. 2005). The model measures the capacity of the bed at different breakthrough values (Vijayaraghavan et al. 2004). It is also one

Table 2 The linear form of various models and the mathematical models for finding breakthrough curves

Model	Mathematical form of equation	Equation for finding breakthrough curve
1. Thomas model	$ln\left(\frac{C_t}{C_o}-1\right)=\left(\frac{k_{Th}q_{eq}m}{F}-k_{Th}C_o t\right)$	$\frac{C_t}{C_o}=\frac{1}{1+\exp\left(\frac{k_{Th}q_{eq}m}{F}-k_{Th}C_o t\right)}$
2. Adams-Bohart model	$\ln\left(\frac{C_t}{C_o}\right)=k_{AB}C_o t-\frac{k_{AB}N_o z}{v}$	$\left(\frac{C_t}{C_o}\right)=\exp\left(k_{AB}C_o t-\frac{k_{AB}N_o z}{v}\right)$
3. Yoon-Nelson model	$\ln\left(\frac{C_t}{C_t-C_o}\right)=k_{YN}t-k_{YN}\tau$	$\frac{C_t}{C_o}=e^{\frac{(k_{YN}t-k_{YN}\tau)}{e}(k_{YN}t-k_{YN}\tau)}+1$
4. Modified dose–response model	$\ln\left(\frac{C_o}{C_t}-1\right)=a\ln b-a\ln(F^*t)$	$\frac{C_t}{C_0}=1-\frac{1}{1+(F^*t/b)^a}$
5. LDFC model	$t=t_o+\frac{\rho_b q_o/C_o}{k_f}(1-Rln(1-x)\frac{-lnx}{1-R})$	$\frac{k_f}{\rho_b q_o/C_o}(t-t_o)=(1-Rln(1-x)\frac{-lnx}{1-R})$
6. LDFQ model	$t=t_o+\frac{\rho_b}{k_s}\left(\frac{R}{1-R}\ln x-\frac{1}{1-R}\ln(1-x)-1\right)$	$\frac{k_s}{\rho_b}(t-t_o)=\frac{R}{1-R}\ln x-\frac{1}{1-R}\ln(1-x)-1$

of the important models for predicting adsorber performance (Prakash Kumar et al. 2005; Chowdhury and Saha 2013). The linear form of this model is given by the relation

$$t=\frac{N_o z}{C_o v}-\frac{1}{K_a C_o}\ln\left(\frac{C_o}{C_b}-1\right) \tag{18}$$

where C_0 is the initial phenol concentration (mg L^{-1}); C_b is the breakthrough phenol concentration (mg L^{-1}); N_o is the sorption capacity of bed per unit bed volume (mg L^{-1}); υ is the linear velocity (cm min^{-1}); and K_a is the rate constant (L/(mg^{-1} h^{-1}). The sorption capacity N_o and the rate constant K_a are determined from the slope and the intercept of the linear plot (Gokhale et al. 2009).

The model parameters can be helpful to predict the service time for other operating conditions without further experimental studies and analysis (Prakash Kumar et al. 2005; Hadi et al. 2011; Saha and Sarkar 2015). The model was also used to evaluate the design parameters for changed flow rate and initial concentration. The column design parameters estimated from Eq. (18) can be used for the practical design of adsorption column.

The simplified form of the model can be given as:

$$t=a\times z-b \tag{19}$$

$$a=\frac{N_o}{C_o F} \tag{20}$$

$$b=\frac{1}{K_a C_o}\ln\left(\frac{C_o}{C_b}-1\right) \tag{21}$$

From the model, if a value is found for one flow rate, values for other flow rates can be obtained. The slope constant (a') for a different flow rate (F') can be calculated by:

$$a'=a\times\frac{F}{F'} \tag{22}$$

where a and F are the old slope and old flow rate, respectively; and a' and F' are the new slope and new flow rate. For other phenol concentration, the desired equation is given by a new slope, and a new intercept by:

$$a' = a \times \frac{C_o}{C'_o} \tag{23}$$

$$b' = b \times \frac{C_o}{C'_o} \times \frac{\ln\left(\frac{C'_o}{C'_b} - 1\right)}{\ln\left(\frac{C_o}{C_b} - 1\right)} \tag{24}$$

where b', b are the new and old intercepts, respectively; C'_o and C_o are the new and old phenol initial concentrations, respectively; and C'_b and C_b are the new and old phenol breakthrough concentrations, respectively (Han et al. 2009).

2.4 The Error Analysis

To find the best fit model for the adsorption process, error analysis was also performed. The error functions used for are the following.

The Chi square statistic test (χ^2) (Chowdhury and Saha 2013)

$$\chi^2 = \sum_{i=1}^{n} \left(\frac{\left(\left(\frac{C_t}{Co}\right)_{i,cal} - \left(\frac{C_t}{Co}\right)_{i,exp} \right)^2}{\left(\frac{C_t}{Co}\right)_{i,exp}} \right) \tag{25}$$

and the least square of errors (SSE) (Mishra et al. 2013)

$$SSE = \sum_{i=1}^{n} \left(\left(\left(\frac{C_t}{Co}\right)_{i,cal} - \left(\frac{C_t}{Co}\right)_{i,exp} \right)^2 \right) \tag{26}$$

where $\left(\frac{C_t}{Co}\right)_{cal}$ and $\left(\left(\frac{C_t}{Co}\right)_{exp}\right.$ are the calculated and the experimental dimensionless concentration values.

3 Materials and Methods

3.1 Preparation of Chemically Treated Carbon

The material *Lantana camara* was washed with distilled water several times to remove all foreign matter. The materials were initially dried in sunlight for 48 h, cut into pieces, grounded to powder, and sieved to several particle sizes ranging from less than 0.075 mm. The proximate analysis of the raw powder was done. It was found the fixed carbon content was 41.4 % as described in the previous work (Girish and Ramachandra Murty 2014). In order to improve the properties of the raw powder, various chemicals such as H_3PO_4, KNO_3, H_2SO_4, $ZnCl_2$, HCl and KOH were used for chemical treatment

as reported by Girish and Ramachandra Murty (2014). The characterisation of the carbon treated with the above chemicals was performed. Various parameters like surface area, pore volume, particle size and percent removal of phenol were measured. Based on the preliminary results, as discussed in the previous work (Girish and Ramachandra Murty 2014), the best adsorbent treated with HCl was used for column studies.

3.2 Chemicals

Phenol has a chemical formula C_6H_5OH with a molecular weight of 94 g/mol and is used as adsorbate. Phenol of analytical grade (Merck India Ltd) was used for the preparation solutions of varying concentration of 100, 150 and 250 mg L^{-1}. The other chemical, Hydrochloric acid (SD Fine Chemicals, India, AR grade), was used for the chemical treatment of carbon.

3.3 Packed-Bed Adsorption Experiments

The packed bed experiments were conducted in a glass column of 2 cm inner diameter and 50 cm height. The adsorbent material was placed between two supporting layers of glass wool, followed by glass beads and then finally closed on both the ends by a sieve. A layer of glass wool was packed to avoid any loss of adsorbent material; the glass beads were placed to provide uniformly distributed flow, and a stainless steel sieve to give mechanical support. The column was packed with 3, 5.93 and 9.28 g of the carbon treated with HCl to obtain a bed height equivalent of 5, 10 and 15 cm. The schematic diagram of the experimental setup is shown in Fig. 1. The effect of operating parameters such as bed height (5, 10 and 15 cm), initial phenol concentration (100, 150 and 250 mg L^{-1}) and flow rate (10, 15 and 20 mL min^{-1}) on the adsorption process through the bed was examined. The phenol solution of known concentration was pumped upwards to the column through a peristaltic pump (EnerTech) at a desired flow rate. The samples at the exit of the column were collected at regular period of time. The concentration of the samples was measured using a double beam UV-visible spectrophotometer (Shimadzu, Japan) at 270 nm. All the experiments were

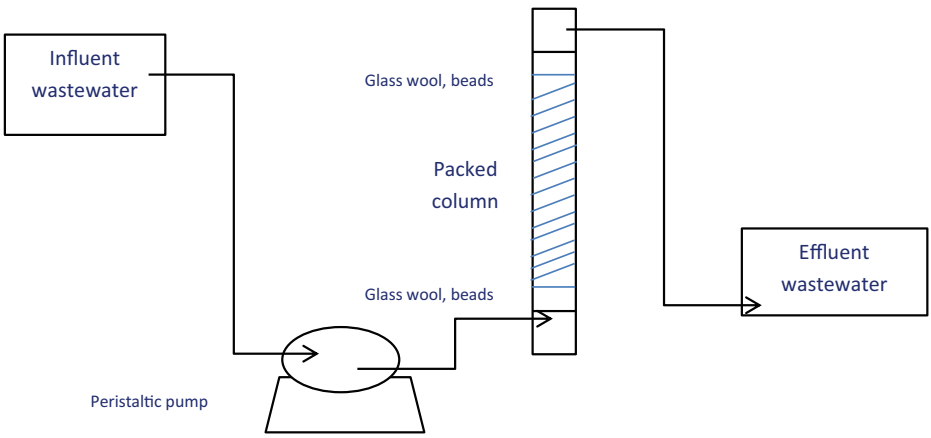

Fig. 1 The schematic representation of experimental setup

conducted at room temperature of 28° C and the pH was maintained at 7.5. The experiment was continued further till the inlet and outlet phenol concentration became constant.

4 Results and Discussion

4.1 Effect of Operating Conditions

4.1.1 Effect of Initial Concentration

The effect of initial phenol concentration on the adsorption was investigated by varying the concentration in the range of 100, 150 and 250 mg L^{-1}, while the bed height and flow rate were kept constant at 10 cm and 15 mL min^{-1}, respectively. The breakthrough curves for different concentrations are shown in Figs. 2 and 3. The experimental values of total quantity of phenol adsorbed, phenol uptake, breakthrough time, exhaustion time, volume of the effluent treated, percent removal, length of mass transfer zone, fractional bed utilization and the value of slope of breakthrough curve are shown in Table 3.

It was noticed that the breakthrough time decreased with increasing concentration. As the concentration increased, the breakthrough curves became steeper, while the broader curves were obtained at lower concentration values. The slope of the curves increased at higher initial concentration. This was due to the fact that the mass transfer driving force increases with increase in phenol concentration (Banat et al. 2007). From these results, it can be understood that the change of concentration gradient influences the saturation rate and breakthrough time (Aksu and Gönen 2004). It can also be inferred that because of the concentration difference formed, the adsorption capacity and % removal increases with increase in phenol concentration (Tamez Uddin et al. 2009). The adsorption capacity and percent removal signifies the extent to which active sites are occupied during the adsorption.

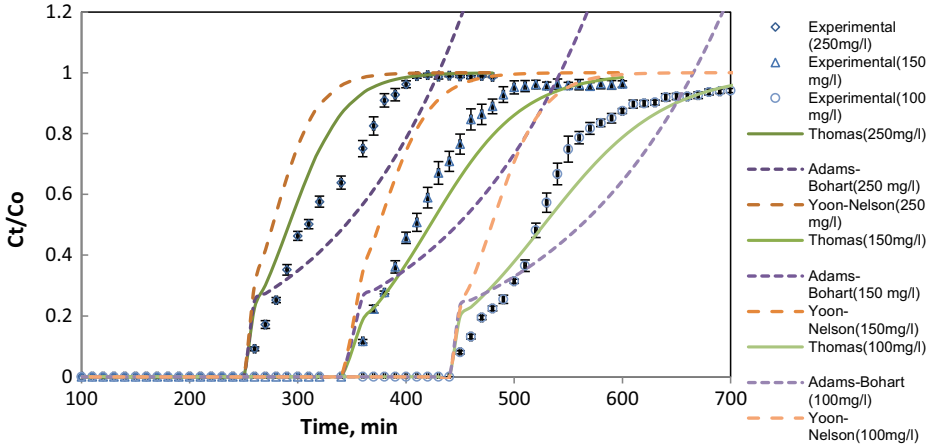

Fig. 2 The prediction of breakthrough curves obtained at different initial phenol concentration from the Thomas, Adams-Bohart and Yoon-Nelson model (10 cm bed height, initial concentration 200 mg L^{-1})

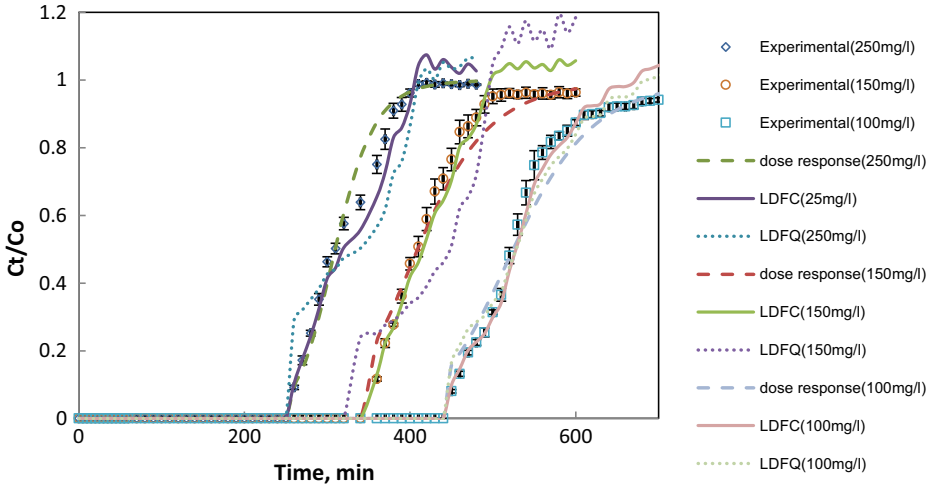

Fig. 3 The prediction of breakthrough curves obtained at different initial phenol concentration from the Modified dose–response, LDFC and LDFQ model (10 cm bed height, initial concentration 200 mgL^{-1})

The steepness of curves determines the column efficiency to reach saturation. The steeper curves have longer mass transfer zone which is necessary for the better column performance (Naja and Volesky 2008; Cruz-Olivares et al. 2013). The total volume of the effluent treated and the fractional bed utilization was more at lower concentration because the reason for this is that at lower concentration the feed solution flows inside the column for a longer residence time. From these results, it can be concluded that the higher concentration of phenol (250 mg L^{-1}) provides better results. But by looking into the system conditions and the concentration of real wastewater as given in Table 1 (Polat et al. 2006; Ucun et al. 2010), the concentration of 150 mg L^{-1} was used for the further experiments. Similar results were reported by Han et al. (2009), Sotelo et al. (2013a), Mitra et al. (2014), Long et al. (2014).

4.1.2 Effect of Flow Rate

The effect of flow rate on phenol removal by carbon was studied by varying the flow rate in the range of 10, 15 and 20 mL min^{-1}, while the bed height and initial phenol concentration were held constant at 10 cm and 150 mg L^{-1}, respectively. The breakthrough curves obtained by plotting effluent phenol concentration versus time at different flow rates are represented in Figs. 4 and 5.

As the flow rate increased, the breakthrough curves became steeper and the slope of the breakthrough curve increased. The possible reason for this can be that as the flow rate increases, the residence time of the adsorbate in the column decreases, which leads to the early exit of the phenol solution from the column. From Table 3, it can be noticed that the breakthrough time, exhaustion time, percent removal, volume treated and uptake capacity decreased as the flow rate increased (Vijayaraghavan et al. 2004; Ahmad and Hameed 2010). With the increase in flow rate, the length of the mass transfer zone increases leading to faster saturation of the column (Ahmad and Hameed 2010). The mass transfer zone also explains how fast the saturation concentration is reached in the packed column. From this, it can be inferred that the higher the mass transfer zone value, the faster the saturation of the bed.

Table 3 Column data and parameters obtained at different operating conditions

Z (cm)	*Co (mg L^{-1})*	*F (mL min^{-1})*	q_{total} *(mg)*	q_{eq} *(mg g^{-1})*	q_b *(mg g^{-1})*	q_s *(mg g^{-1})*	% rem	*MTZ (cm)*	*FBU*	*dc/dt (mg L^{-1} min^{-1})*	*Veff (L)*
5	150	15	391.95	130.65	28.74	379.4	75.73	2.2258	0.067844	1.17198	2.0641
10	150	15	887.61	149.68	58.545	785	81.3	2.737	0.07458	0.90361	5.286
15	150	15	1302.10	152.292	119.88	1262.5	83.1	2.899	0.094949	0.8811	8.4315
10	100	15	739.377	124.68	57.51	695.74	78.3	2.611	0.082659	0.4866	6.9765
10	250	15	1172.34	197.696	74.884	1056.4	83.36	3.0378	0.07084	1.511	3.9193
10	150	10	1014.42	171.06	94.09	954.53	82.58	2.2517	0.098572	0.6507	6.3452
10	150	20	757.12	127.67	58.66	697.79	81.15	3.5349	0.069161	1.0916	4.0207

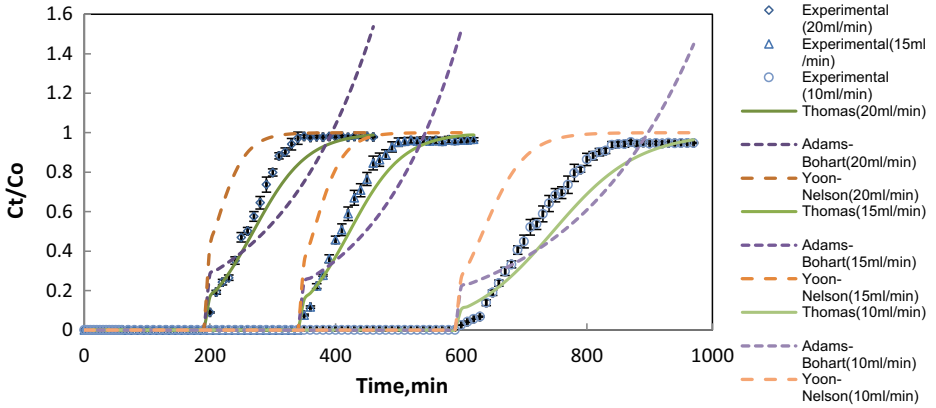

Fig. 4 The prediction of breakthrough curves obtained at different flow rates from the Thomas, Adams-Bohart and Yoon-Nelson model (15 mL/min flow rate, initial concentration 200 mg L^{-1})

Finally, at low rate of influent, the residence time of phenol in contact with the adsorbent is higher, which results in a higher percent removal and more uptake of phenol (Han et al. 2009; Chen et al. 2012). It can be concluded that best results were obtained at the lowest flow rate of 10 mL min^{-1}. But by looking into the longer breakthrough time required and the higher energy cost associated, the flow rate of 15 mL min^{-1} was chosen for the subsequent experiments. Similar results have been reported by other researchers (Ahmad and Hameed 2010; Mitra et al. 2014; Chen et al. 2012; Long et al. 2014).

4.1.3 Effect of Bed Height

The column behaviour for phenol adsorption with different bed heights of 5, 10 and 15 cm was investigated with inlet phenol concentration of 150 mg L^{-1} and a flow rate of 15 mL min^{-1}. Figures 6 and 7 indicates the breakthrough profile at different bed heights. The breakthrough time, exhaustion time, uptake capacity, percent removal, volume treated increased with the increase in bed height and are presented in Table 3. It was also noticed that the slope of

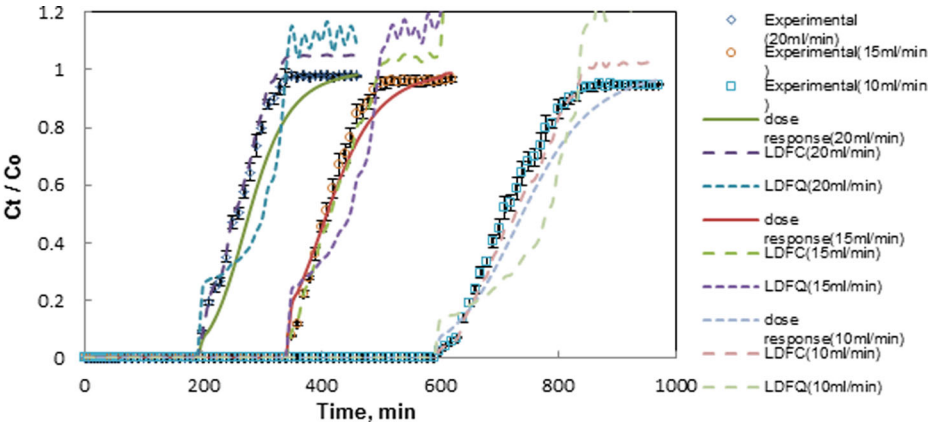

Fig. 5 The prediction of breakthrough curves obtained at different flow rates from the Modified dose–response, LDFC and LDFQ model (15 mL/min flow rate, initial concentration 200 mg L^{-1})

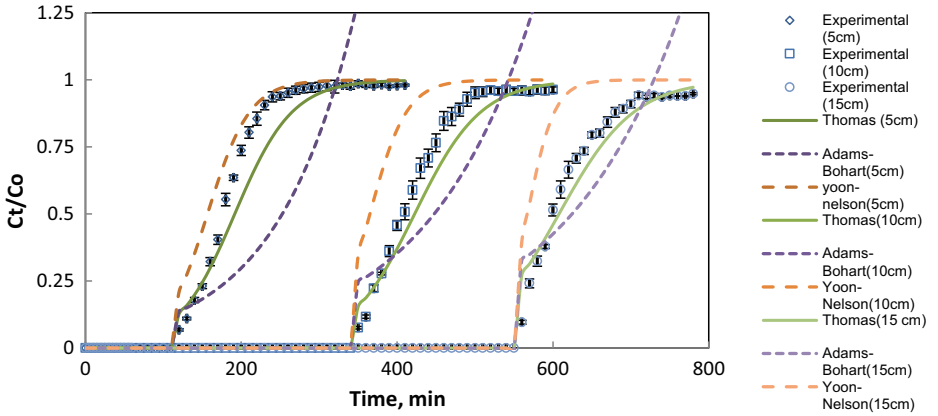

Fig. 6 The prediction of breakthrough curves obtained at different bed heights from the Thomas, Adams-Bohart and Yoon-Nelson model (15 mL/min flow rate, initial concentration 200 mg L^{-1})

breakthrough curve decreased with increasing bed height; thus, it results in a extended mass transfer zone (Ahmad and Hameed 2010). This was due to the fact that with increasing bed height, more binding sites are available for adsorbate to diffuse through the pores of the adsorbent and the adsorption area increases (Tamez Uddin et al. 2009; Lezehari et al. 2012; Gupta and Babu 2009; Baral et al. 2009). The breakthrough time in shorter bed is generally lower and complete utilization of the bed may not be possible (Sotelo et al. 2013b). Considering the adsorption capacity and the other results at different bed heights, 10 cm bed height was selected for further experiments. Similar results have been reported by other researchers (Vijayaraghavan et al. 2004; Tamez Uddin et al. 2009; Chen et al. 2012; Mitra et al. 2014).

4.2 Modelling of the Breakthrough Curves

In this study, Thomas, Modified dose–response, Yoon-Nelson, Adams-Bohart, Clark, LDFC and LDFQ model were used for predicting the dynamic behaviour of the column.

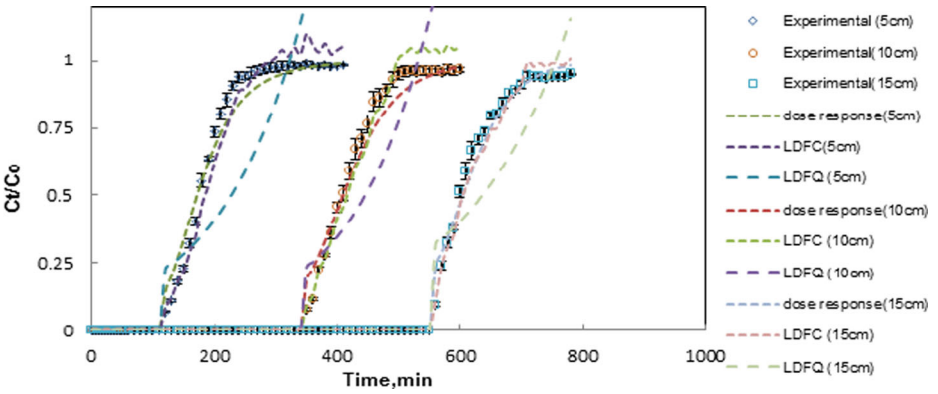

Fig. 7 The prediction of breakthrough curves obtained at different bed heights from the Modified dose–response, LDFC and LDFQ model (15 mL/min flow rate, initial concentration 200 mg L^{-1})

Table 4 The Thomas model parameters obtained at different experimental conditions

Z (cm)	Co (mg L^{-1})	F (mL min^{-1})	k_{Th} (mL mg^{-1} min^{-1})	$q_{eq,\ th}$ (mg g^{-1})	$q_{eq,\ exp}$ (mg g^{-1})	R^2	χ^2	SSE
5	150	15	0.1795±0.00393	132.72±0.8549	130.65	0.9699	0.0187	0.0061
10	150	15	0.1566±0.01193	155.47±2.41	149.68	0.9786	0.0106	0.0031
15	150	15	0.1382±0.00206	159.45±1.1779	152.292	0.9708	0.0140	0.00406
10	100	15	0.1843±0.00262	133.4±0.9063	124.68	0.9716	0.0135	0.0054
10	250	15	0.1333±0.0083	194.54±1.1361	197.69	0.9807	0.0827	0.0012
10	150	10	0.1179±0.0226	180.72±2.9711	171.06	0.9635	0.0256	0.0036
10	150	20	0.164±0.0016	124.55±4.9430	127.67	0.9941	0.0104	0.0029

4.2.1 Thomas Model

As shown in Table 4, the value of q_{eq} increased and the value of k_{Th} decreased with the increase in initial phenol concentration. This may happen because of the driving force required for adsorption increases with increase in concentration (Han et al. 2006). As presented in Table 4, with increase in flow rate, the maximum adsorption capacity q_{eq} decreased and k_{Th} increased. It was also noticed that increasing bed height, the values of q_{eq} increased while the value of k_{Th} decreased. From all these it can be concluded that lower flow rate, higher initial concentration and higher bed height resulted in better column performance. From Figs. 2, 4 and 6, it can be seen that the experimental values and the predicted values by Thomas model are closer for all the experimental conditions. The regression coefficient is higher than 0.9635 which shows the validity of the model for all conditions. The value of χ^2 is less than 0.02 and SSE values less than 0.006 show the good matching of experimental and theoretical values. This shows that the model predicts well the adsorption process. The model is generally used in describing the processes where internal diffusion is not the rate determining step (Aksu and Gönen 2004; Chen et al. 2012). A similar trend has been reported by Song et al. (2011), Mitra et al. (2014), Singha et al. (2012) for the adsorption of phenol.

4.2.2 Adams-Bohart Model

The values of k_{AB} and N_o were calculated and are presented in Table 5, along with the correlation coefficients (R^2). It was found that the adsorption capacity of the bed (N_o) decreased

Table 5 The Adams-Bohart model parameters obtained at different experimental conditions

Z (cm)	Co(mg L^{-1})	F (mL min^{-1})	$k_{AB}\times10^{-3}$ (L mg^{-1} h^{-1})	N_o (mg mL^{-1})	R^2	χ^2	SSE
5	150	15	0.0511±0.001	44.19±0.6790	0.8091	0.2659	0.2270
10	150	15	0.04888±0.0012	38.74±0.2614	0.7839	0.0752	0.3303
15	150	15	0.0440±0.0018	34.93±0.2083	0.7760	0.0478	0.0373
10	100	15	0.0666±0.0016	31.99±0.1488	0.7837	0.0738	0.0584
10	250	15	0.0325±0.0013	51.61±0.4221	0.8400	0.0540	0.0450
10	150	10	0.0319±0.0019	42.43±0.35781	0.8091	0.0664	0.0427
10	150	20	0.0503±0.0031	34.84±0.1284	0.7760	0.0681	0.0564

with increase in flow rate and bed height, but increased with increase in concentration. In addition, the parameter k_{AB} increased with increasing flow rate and decreased with increasing concentration and bed height. Using the above model, the predicted breakthrough curves were obtained and are shown in Figs. 2, 4 and 6. From the breakthrough curve, it can be observed that a linear relationship exists between C_t/C_o and t for the relative concentration range up to 0.25 (Aksu and Gönen 2004). The value of χ^2 and SSE obtained were less than 0.2659 and 0.3303, respectively. This also demonstrates that the kinetics was controlled by external mass transfer in the initial part of adsorption process (Ahmad and Hameed 2010). Similar observations have been made by Long et al. (2014), Aksu and Gönen (2004) and Mitra et al. 2014.

4.2.3 Yoon-Nelson Model

The values of k_{YN} and τ obtained from the Yoon-Nelson model are presented in Table 6. It was found that with the flow rate and phenol influent concentration increasing, the values of k_{YN} increased and the breakthrough time τ decreased. The reason for this may be that the decrease in the value of τ leads to the faster saturation of the bed (Chen et al. 2012). The increase in k_{YN} with flow rate shows a decrease in the mass transfer resistance, and thus, an increase in the driving force required for the mass transfer in the liquid film (Mitra et al. 2014). With the bed height increasing, the values of τ increased while the values of k_{YN} decreased. It can also be observed from Table 6 that the calculated τ values were significantly deviating from the experimental values ($t_{,exp}$). The comparison of the experimental curves and the theoretical curves are also represented in Figs. 2, 4 and 6. The experimental curves were slightly closer to the predicted curves at the higher values of concentration and flow rate and lower values of bed height. From the value of R^2 ranging from 0.91 to 0.93 and χ^2 and SSE values, it is confirmed that the model provides a poor fit to the experimental data. Thus from the results, it can be confirmed that the experimental results provided poor fit of the model. A similar dependency has also been observed by other researchers (Long et al. 2014; Aksu and Gönen 2004; Han et al. 2009).

4.2.4 Modified Dose–Response Model

The predicted breakthrough curves from the Modified dose–response model are shown in Figs. 3, 5 and 7. The model replicates the experimental results for the various concentration values (Martín-Lara et al. 2010). The parameters a and b obtained from the model are summarised in Table 7. It was noted from the results that the constant a increased with increasing bed height and initial

Table 6 The Yoon-Nelson model parameters obtained at different experimental conditions

Z (cm)	*Co, (mg L^{-1})*	*F (mL min^{-1})*	*k_{YN} (min^{-1})*	*τ (min)*	*$t_{,exp}$ (min)*	*R^2*	*χ^2*	*SSE*
5	150	15	0.0278±0.0007	156.74±3.39	176.4	0.9104	0.1194	0.0058
10	150	15	0.0235±0.0179	431.13±7.65	408.42	0.9435	0.10171	0.0031
15	150	15	0.0207±0.0003	579.5±5.74	598.92	0.9295	0.0430	0.0040
10	100	15	0.0184±0.0002	499.12±8.01	522.03	0.9378	0.08235	0.0054
10	250	15	0.0333±0.0020	296.81±3.67	309.1	0.9362	0.3031	0.0012
10	150	10	0.0155±0.0002	685.08±8.59	707.12	0.9215	0.25826	0.0066
10	150	20	0.0288±0.0009	237.27±8.93	260.0	0.9176	0.1344	0.0029

Table 7 The Modified dose–response model parameters obtained at different experimental conditions

Z (cm)	*Co, (mg L^{-1})*	*F (mL min^{-1})*	*a*	*b (mL)*	$q_{eq,exp}$ *(mg g^{-1})*	$q_{eq,th}$ *(mg g^{-1})*	R^2	χ^2	*SSE*
5	150	15	5.69±0.1570	2573.2±26.49	130.65	128.66	0.9899	0.0048	0.0021
10	150	15	11.17±0.8402	6135.98±79.44	149.68	155.21	0.9898	0.0057	0.0014
15	150	15	13.98±0.196	9068.4±60.42	152.29	159.09	0.9850	0.0140	0.0028
10	100	15	10.91±0.1817	7868.75±62.56	132.69	124.68	0.9831	0.0080	0.0035
10	250	15	12.10±0.7561	4643.09±52.52	195.74	197.69	0.9889	0.0446	0.0054
10	150	10	12.45±0.2083	7138.35±76.84	180.56	171.06	0.9814	0.0169	0.0019
10	150	20	4.96±0.0535	5014.88±54.59	126.85	127.67	0.9842	0.0284	0.0013

concentration but decreased with increasing flow rate. The theoretical values of q_{eq} obtained from dose response model were more similar to the experimental values, than the theoretical values of q_{eq} obtained from the Thomas model. Values of χ^2 less than 0.01 and SSE less than 0.005 show that experimental values are in closer agreement with the calculated values. The value of R^2 ranged from 0.9814 to 0.9899, showing that the experimental results provide a better fit of this model than the Thomas model. Other authors have published similar results (Mishra et al. 2013; Park et al. 2014; Zhao et al. 2010).

4.2.5 LDFC Model

Using the model equation, the breakthrough time (t_o), equilibrium parameter *(R)* and the model parameters were determined and are shown in Table 8. The experimental and the predicted breakthrough curves determined for different experimental conditions are shown in Figs. 3, 5 and 7. It was observed that as the bed height increased, the breakthrough time (t_o) increased, and the mass transfer coefficient (k_f) decreased. The reason for this behaviour can be discussed on the basis that the mass-transfer zone in the initial region of the bed enlarges, and then proceeds as a stable zone (Lua and Jia 2009). With the initial concentration increasing, the breakthrough time (t_o) decreased. The probable reason for this is that higher concentration contributes to higher driving force to overcome all mass transfer resistances (Sharma and singh 2013). Thus, the mass-transfer coefficient increases with increase in initial concentration because the mass transfer zone at higher concentration proceeds faster than at lower concentration (Zhang et al. 2011). When the flow rate increased from 10 to 20 mL min^{-1}, the breakthrough time decreased. The probable reason behind

Table 8 The LDFC model parameters obtained at different experimental conditions

Z (cm)	*Co, (mg L^{-1})*	*F (mL min^{-1})*	k_f *(min^{-1})*	t_o *(min)*	*R*	R^2	χ^2	*SSE*
5	150	15	1.091±0.034	218.22±25.84	0.14444	0.9825	0.0056	0.1516
10	150	15	0.5587±0.016	423.79±5.39	0.14444	0.9845	0.0592	0.0037
15	150	15	0.3278±0.0063	612.14±4.41	0.14444	0.9893	0.0026	0.0477
10	100	15	0.5306±0.0047	537.21±3.504	0.2020	0.9806	0.0040	0.0035
10	250	15	0.5792±0.0043	319.22±4.639	0.09193	0.9852	0.0446	0.0037
10	150	10	0.3827±0.0034	729.06±4.632	0.14444	0.9894	0.0050	0.0037
10	150	20	0.5892±0.0085	210.58±3.9868	0.14444	0.9899	0.0284	0.0001

this is that high flow rate reduces the boundary layer thickness around the carbon surface, thus, the external mass-transfer resistance decreases, the breakthrough time decreases and the mass transfer coefficient increases (Zhang et al. 2010). Analysis of the regression coefficients indicated that the regressed lines provided excellent fits to the experimental data with R^2 values ranging from 0.9806 to 0.9899. The values of χ^2 less than 0.0292 and of SSE less than 0.0477 indicate that the experimental results fit well with this model.

4.2.6 LDFQ Model

Using the LDFQ model equation, the theoretical breakthrough curves were plotted and are shown in Figs. 3, 5 and 7. The parameters of the LDFQ model are listed in Table 9. It was noticed that when increasing the bed height the breakthrough time increased. The mass transfer zone in a packed bed moves from the entrance and then advances towards the exit. Therefore, increasing the bed height, decreases the time required for the mass transfer zone to reach the exit (Singh et al. 2008). The effect of initial concentration of phenol (100, 150 and 250 mg L^{-1}) on breakthrough was studied. It was found that as the phenol concentration increases the time required for bed saturation decreases (Leyva-Ramos et al. 2007). Therefore, as the influent concentration increases the breakthrough curve becomes steeper. For a low flow rate, the time required for breakthrough is lower when compared to the time required for high flow rate. Therefore, as the flow rate increases, the mass transfer increases resulting in faster saturation of the bed. From the values of regression coefficient, χ^2 and SSE, it can be concluded that large disparities were found between experimental and theoretical values.

4.3 Design of the Column from BDST Model

From the BDST equation, the model parameters were determined and are presented in Table 10. It was noticed that as the C_t/C_b values increased, the values of N_0 increased while *Ka* decreased. The rate constant *Ka* shows the rate of solute transfer from the fluid phase to the solid phase (Aksu and Gönen 2004). If the value of *Ka* increases, short bed may be sufficient to prevent breakthrough. But if *Ka* value decreases, then a long bed may be required to prevent breakthrough (Vijayaraghavan et al. 2004). The increase in N_0 shows the presence of larger mass transfer driving force (Banat et al. 2007).

Table 9 The LDFQ model parameters obtained at different experimental conditions

Z (cm)	*Co, (mg L^{-1})*	*F (mL min^{-1})*	*k_s (min^{-1})*	*t_o (min)*	*R*	*R^2*	*χ^2*	*SSE*
5	150	15	0.0055±0.0002	181.3±1.93	0.14444	0.6790	0.1428	0.133
10	150	15	0.0050±0.0006	417.25±5.15	0.14444	0.8868	0.0494	0.0807
15	150	15	0.004±0.0005	616.35±3.26	0.14444	0.8175	0.0546	0.0305
10	100	15	0.0041±0.0004	532.94±4.20	0.2020	0.8995	0.0075	0.0772
10	250	15	0.0051±0.0037	319.46±1.49	0.09193	0.9384	0.0245	0.0373
10	150	10	0.0033±0.00015	727±6.03	0.14444	0.8767	0.0934	0.0526
10	150	20	0.0047±0.00027	181±1.37	0.14444	0.8854	0.0569	0.0307

Table 10 The BDST parameters at different breakthrough values

C_t/C_b	*a (min cm^{-1})*	*b (min)*	*No (mg L^{-1})*	*Ka (L mg^{-1} min^{-1})*
0.1	43.267	84.737	30983.5	1.73×10^{-4}
0.2	41.605	54.013	29793.34	1.46×10^{-4}
0.3	41.95	47.043	30040.4	1.20×10^{-4}
0.4	42.005	37.02	30079.78	0.073×10^{-4}

The parameters evaluated at experimental conditions of 150 mg L^{-1} and flow rate of 15 mL min^{-1} were employed to predict the design parameters at other experimental conditions (flow rate of 10 mL min^{-1}, 20 mL min^{-1} and initial concentration of 100 and 250 mg L^{-1}). The predicted time (t_c) and the experimental time (t_e) for different values of flow rate and initial concentration were found. Also, the percent values of error (E) between them are presented in Table 11. It was noticed from Table 11 that the calculated and experimental service time were well close to each other. These findings also show that the model can be used for the design of adsorber performance at other operating conditions. These results are in good agreement with those referred by other authors (Han et al. 2009; Zhao et al. 2010; Chan et al. 2012).

The plot of bed height versus service time for 10 % and 90 % saturation of the column were made. From Fig. 8, the BDST equations were used to determine the length of mass transfer zone.

Table 11 The prediction of BDST parameters at other flow rate and initial concentrations

C_t/C_b	*a^1 (min cm^{-1})*	*b^1 (min)*	*tc (min)*	*te (min)*	*E (%)*
10 mL/min, 150 mg L^{-1}					
0.1	64.9	84.737	564.263	634	12.359
0.2	63.45	63.347	571.153	652	14.155
0.3	62.925	47.043	582.207	678.2	16.488
0.4	63.0075	37.02	593.055	689.2	16.212
20 mL/min, 150 mg L^{-1}					
0.1	32.445	84.737	239.713	201.039	16.1335
0.2	31.72	63.347	253.853	211.578	16.6533
0.3	31.4625	47.043	267.582	234.06	12.5277
0.4	31.5037	37.02	278.017	244.06	12.214
15 mL/min, 100 mg L^{-1}					
0.1	64.9	127.105	521.895	454.26	12.9595
0.2	63.45	95.02	539.48	471.77	12.551
0.3	62.925	70.56	558.69	497.63	10.9291
0.4	63.0075	55.53	574.545	512.98	10.7154
15 mL/min, 250 mg L^{-1}					
0.1	25.956	50.84	208.72	261	25.048
0.2	25.383	38.008	215.822	273.5	26.725
0.3	25.17	28.22	223.48	284.8	27.439
0.4	25.203	22.212	229.818	294.31	28.062

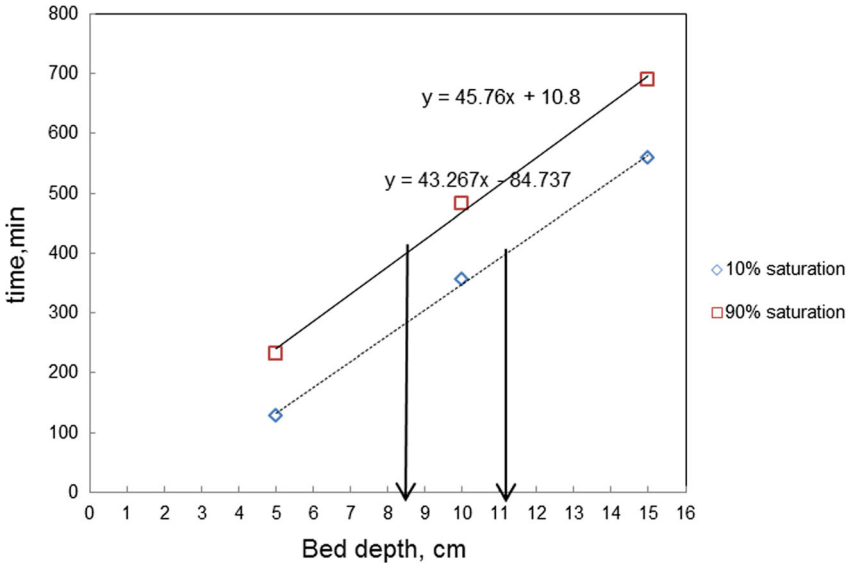

Fig. 8 Prediction of length of mass transfer zone from BDST curve

Since the values of slope of both lines were almost the same, the lines are parallel to each other. Therefore, the horizontal distance between the two lines, which gives the length of mass transfer zone was 2.75 cm. The experimental value was found to be 2.548 cm. These results are similar to those reported by Yousef and El-Eswed (2009).

5 Conclusion

The problem of disposing the poisonous forest waste *Lantana camara* has been resolved by utilizing it as an effective adsorbent for removal of phenol from aqueous solutions in a packed-bed column. The adsorbent showed the best performance with an adsorption capacity of 149.77 mg g^{-1}. The process can be considered as industrially feasible since the adsorbent can treat wastewater of industrial standard. The influence of various operating parameters, such as flow rate, bed height and initial phenol concentration were investigated. The adsorption capacity increased with increasing bed depth and influent concentration but decreased with increasing flow rate. The Thomas, Adams-Bohart, Yoon–Nelson, Modified dose - response, LDFC and LDFQ models were applied to the column data to predict the breakthrough curve and to determine the adsorption capacity of the column. The Thomas and LDFC models were found to be most suitable in fitting the experimental data for the packed-bed system. From the experimental findings, the Thomas model was capable of describing the column adsorption which suggests that the process was controlled by interface mass transfer. Modelling column data also resulted in good agreement with the LDFC model which shows that the fluid phase concentration difference is the driving force for adsorption. The BDST design model was employed to design the adsorption column for other values of flow rate and initial concentration. The model was also capable of depicting the column performance for the adsorption of phenol from aqueous solution. Finally, it can be concluded that the present work

is addressing two environmental problems, i.e., treatment of wastewater and handling the invasive forest waste.

Compliance with ethical standard

Conflict of Interest The authors declare that they have no conflict of interest.

References

Adak A, Pal A (2006) Removal of phenol from aquatic environment by SDS-modified alumina: batch and fixed bed studies. Sep Purif Technol 50(2):256–262

Ahmad AA, Hameed BH (2010) Fixed-bed adsorption of reactive azo dye onto granular activated carbon prepared from waste. J Hazard Mater 175(1):298–303

Aksu Z, Gönen F (2004) Biosorption of phenol by immobilized activated sludge in a continuous packed bed: prediction of breakthrough curves. Process Biochem 39(5):599–613

An F, Feng X, Gao B (2009) Adsorption of aniline from aqueous solution using novel adsorbent PAM/SiO_2. Chem Eng J 151(1):183–187

Auta M, Hameed BH (2014) Chitosan–clay composite as highly effective and low-cost adsorbent for batch and fixed-bed adsorption of methylene blue. Chem Eng J 237:352–361

Banat FA, Al-Asheh S (2000) Biosorption of phenol by chicken feathers. Environ Eng Policy 2(2):85–90

Banat F, Al-Asheh S, Al-Ahmad R, Bni-Khalid F (2007) Bench-scale and packed bed sorption of methylene blue using treated olive pomace and charcoal. Bioresour Technol 98(16):3017–3025

Baral SS, Das N, Ramulu TS, Sahoo SK, Das SN, Chaudhury GR (2009) Removal of Cr (VI) by thermally activated weed Salvinia cucullata in a fixed-bed column. J Hazard Mater 161(2):1427–1435

Chan LS, Cheung WH, Allen SJ, McKay G (2012) Error analysis of adsorption isotherm models for acid dyes onto bamboo derived activated carbon. Chin J Chem Eng 20(3):535–542

Chen S, Yue Q, Gao B, Li Q, Xu X, Fu K (2012) Adsorption of hexavalent chromium from aqueous solution by modified corn stalk: a fixed-bed column study. Bioresour Technol 113:114–120

Chowdhury S, Saha PD (2013) Artificial neural network (ANN) modeling of adsorption of methylene blue by NaOH-modified rice husk in a fixed-bed column system. Environ Sci Pollut Res 20(2):1050–1058

Cruz-Olivares J, Pérez-Alonso C, Barrera-Díaz C, Ureña-Nuñez F, Chaparro-Mercado MC, Bilyeu B (2013) Modeling of lead (II) biosorption by residue of allspice in a fixed-bed column. Chem Eng J 228:21–27

Damjanović L, Rakić V, Rac V, Stošić D, Auroux A (2010) The investigation of phenol removal from aqueous solutions by zeolites as solid adsorbents. J Hazard Mater 184(1):477–484

Danis TG, Albanis TA, Petrakis DE, Pomonis PJ (1998) Removal of chlorinated phenols from aqueous solutions by adsorption on alumina pillared clays and mesoporous alumina aluminum phosphates. Water Res 32(2):295–302

Dutta M, Basu JK (2014) Fixed-bed column study for the adsorptive removal of acid fuchsin using carbon–alumina composite pellet. Int J Environ Sci Technol 11(1):87–96

Dwivedi CP, Sahu JN, Mohanty CR, Mohan BR, Meikap BC (2008) Column performance of granular activated carbon packed bed for Pb (II) removal. J Hazard Mater 156(1):596–603

Førland GM, Blokhus AM (2007) Adsorption of phenol and benzyl alcohol onto surfactant modified silica. J Colloid Interface Sci 310(2):431–435

Girish CR, Ramachandra Murty V (2014) Adsorption of phenol from aqueous solution using *Lantana camara*, forest waste: kinetics, isotherm, and thermodynamic studies. Inter Sch Res Not. Article ID: 201626

Goel J, Kadirvelu K, Rajagopal C, Garg VK (2005) Removal of lead (II) by adsorption using treated granular activated carbon: batch and column studies. J Hazard Mater 125(1):211–220

Gokhale SV, Jyoti KK, Lele SS (2009) Modeling of chromium (VI) biosorption by immobilized *Spirulina platensis* in packed column. J Hazard Mater 170(2):735–743

Gopal N, Asaithambi M, Sivakumar P, Sivakumar V (2014) Adsorption studies of a direct dye using polyaniline coated activated carbon prepared from Prosopis juliflora. J Water Process Eng 2:87–95

Gupta S, Babu BV (2009) Modeling, simulation, and experimental validation for continuous Cr (VI) removal from aqueous solutions using sawdust as an adsorbent. Bioresour Technol 100(23):5633–5640

Hadi M, Samarghandi MR, McKay G (2011) Simplified fixed bed design models for the adsorption of acid dyes on novel pine cone derived activated carbon. Water Air Soil Pollut 218(1–4):197–212

Han R, Wang Y, Zhao X, Wang Y, Xie F, Cheng J, Tang M (2009) Adsorption of methylene blue by phoenix tree leaf powder in a fixed-bed column: experiments and prediction of breakthrough curves. Desalination 245(1):284–297

Han R, Zhang J, Zou W, Xiao H, Shi J, Liu H (2006) Biosorption of copper (II) and lead (II) from aqueous solution by chaff in a fixed-bed column. J Hazard Mater 133(1):262–268
Hartmann J, Beyer R, Harm S (2014) Effective removal of estrogens from drinking water and wastewater by adsorption technology. Environ Process 1(1):87–94
Karnib A (2014) A methodological approach for quantitative assessment of the effective wastewater management: Lebanon as a case study. Environ Process 1(4):483–495
Karunarathne HDSS, Amarasinghe BMWPK (2013) Fixed Bed Adsorption Column Studies for the Removal of Aqueous Phenol from Activated Carbon Prepared from Sugarcane Bagasse. Energy Procedia 34:83–90
Leyva-Ramos R, Diaz-Flores PE, Leyva-Ramos J, Femat-Flores RA (2007) Kinetic modeling of pentachlorophenol adsorption from aqueous solution on activated carbon fibers. Carbon 45(11):2280–2289
Lezehari M, Baudu M, Bouras O, Basly JP (2012) Fixed-bed column studies of pentachlorophenol removal by use of alginate-encapsulated pillared clay microbeads. J Colloid Interface Sci 379(1):101–106
Long Y, Lei D, Ni J, Ren Z, Chen C, Xu H (2014) Packed bed column studies on lead (II) removal from industrial wastewater by modified *Agaricus bisporus*. Bioresour Technol 152:457–463
Lua AC, Jia Q (2009) Adsorption of phenol by oil–palm-shell activated carbons in a fixed bed. Chem Eng J 150(2):455–461
Markovska L, Meshko V, Noveski VV (2001) Adsorption of basic dyes in a fixed bed column. Korean J Chem Eng 18(2):190–195
Martín-Lara MA, Hernáinz F, Blázquez G, Tenorio G, Calero M (2010) Sorption of Cr (VI) onto olive stone in a packed bed column: Prediction of kinetic parameters and breakthrough curves. J Environ Eng 136(12):1389–1397
Melidis P (2015) Fluoride removal from aluminium finishing wastewater by hydroxyapatite. Environ Process 2(1):205–213
Mishra V, Balomajumder C, Agarwal VK (2013) Adsorption of Cu (II) on the surface of nonconventional biomass: a study on forced convective mass transfer in packed bed column. *J Waste Manage.* Article ID: 632163
Mitra T, Singha B, Bar N, Das SK (2014) Removal of Pb (II) ions from aqueous solution using water hyacinth root by fixed-bed column and ANN modelling. J Hazard Mater 273:94–103
Naja G, Volesky B (2008) Optimization of a biosorption column performance. Environ Sci Technol 42(15):5622–5629
Nuić I, Trgo M, Perić MJ, Medvidović NV (2013) Analysis of breakthrough curves of Pb and Zn sorption from binary solutions on natural clinoptilolite. Microporous Mesoporous Mater 167:55–61
Park SJ, Lee CG, Kim SB (2014) Lab-scale experiments and model analyses for bacterial removal in flow-through columns containing dolomite. Desalin Water Treat 52(34–36):6556–6566
Polat H, Molva M, Polat M (2006) Capacity and mechanism of phenol adsorption on lignite. Int J Miner Process 79(4):264–273
Prakash Kumar BG, Miranda LR, Velan M (2005) Adsorption of Bismark Brown dye on activated carbons prepared from rubberwood sawdust (*Hevea brasiliensis*) using different activation methods. J Hazard Mater 126(1):63–70
Priyanka N, Joshi PK (2013) A review of *Lantana camara* studies in India. Int J Sci Res Pub 3(10):42–52
Reza Rahmani A, Hossieni E, Poormohammadi A (2015) Removal of chromium (VI) from aqueous solution using electro-fenton process. Environ Process 2(2):419–428
Saad DM, Cukrowska E, Tutu H (2014) Column adsorption studies for the removal of U by phosphonated cross-linked polyethylenimine: modelling and optimization. Appl Water Sci 5(1):57–63
Saha S, Sarkar P (2015) Arsenic mitigation by chitosan-based porous magnesia-impregnated alumina: performance evaluation in continuous packed bed column. Int J Environ Sci Technol, 1–14
Sharma R, Singh B (2013) Removal of Ni (II) ions from aqueous solutions using modified rice straw in a fixed bed column. Bioresour Technol 146:519–524
Simate GS, Ndlovu S (2015) The removal of heavy metals in a packed bed column using immobilized cassava peel waste biomass. J Ind Eng Chem 21:635–643
Singh KP, Malik A, Sinha S, Ojha P (2008) Liquid-phase adsorption of phenols using activated carbons derived from agricultural waste material. J Hazard Mater 150(3):626–641
Singha S, Sarkar U, Mondal S, Saha S (2012) Transient behavior of a packed column of *Eichhornia crassipes* stem for the removal of hexavalent chromium. Desalination 297:48–58
Song J, Zou W, Bian Y, Su F, Han R (2011) Adsorption characteristics of methylene blue by peanut husk in batch and column modes. Desalination 265(1):119–125
Sotelo JL, Ovejero G, Rodríguez A, Álvarez S, García J (2013a) Study of natural clay adsorbent sepiolite for the removal of caffeine from aqueous solutions: batch and fixed-bed column operation. Water Air Soil Pollut 224(3):1–15
Sotelo JL, Ovejero G, Rodríguez A, Álvarez S, García J (2013b) Analysis and modeling of fixed bed column operations on flumequine removal onto activated carbon: pH influence and desorption studies. Chem Eng J 228:102–113
Su Y, Zhao B, Xiao W, Han R (2013) Adsorption behavior of light green anionic dye using cationic surfactant-modified wheat straw in batch and column mode. Environ Sci Pollut Res 20(8):5558–5568
Tamez Uddin M, Rukanuzzaman M, Maksudur Rahman Khan M, Akhtarul Islam M (2009) Adsorption of methylene blue from aqueous solution by jackfruit (*Artocarpus heteropyllus*) leaf powder: A fixed-bed column study. J Environ Manag 90(11):3443–3450

Tepe O, Dursun AY (2008) Combined effects of external mass transfer and biodegradation rates on removal of phenol by immobilized *Ralstonia eutropha* in a packed bed reactor. J Hazard Mater 151(1):9–16

Tor A, Cengeloglu Y, Aydin ME, Ersoz M (2006) Removal of phenol from aqueous phase by using neutralized red mud. J Colloid Interface Sci 300(2):498–503

Ucun H, Yildiz E, Nuhoglu A (2010) Phenol biodegradation in a batch jet loop bioreactor (JLB): Kinetics study and pH variation. Bioresour Technol 101(9):2965–2971

Vázquez G, Alonso R, Freire S, González-Álvarez J, Antorrena G (2006) Uptake of phenol from aqueous solutions by adsorption in a *Pinus pinaster* bark packed bed. J Hazard Mater 133(1):61–67

Vijayaraghavan K, Jegan J, Palanivelu K, Velan M (2004) Removal of nickel (II) ions from aqueous solution using crab shell particles in a packed bed up-flow column. J Hazard Mater 113(1):223–230

Volesky B, Weber J, Park JM (2003) Continuous-flow metal biosorption in a regenerable *Sargassum* column. Water Res 37(2):297–306

Wang S, Ang HM, Tade MO (2008) Novel applications of red mud as coagulant, adsorbent and catalyst for environmentally benign processes. Chemosphere 72(11):1621–1635

Yoon YH, Nelson JH (1984) Application of gas adsorption kinetics I. A theoretical model for respirator cartridge service life. Am Ind Hyg Assoc J 45(8):509–516

Yousef RI, El-Eswed B (2009) The effect of pH on the adsorption of phenol and chlorophenols onto natural zeolite. Colloids Surf A 334(1):92–99

Zhang X, Chen S, Bi HT (2010) Application of wave propagation theory to adsorption breakthrough studies of toluene on activated carbon fiber beds. Carbon 48(8):2317–2326

Zhang X, Zhao X, Hu J, Wei C, Bi HT (2011) Adsorption dynamics of trichlorofluoromethane in activated carbon fiber beds. J Hazard Mater 186(2):1816–1822

Zhao L, Zou W, Zou L, He X, Song J, Han R (2010) Adsorption of methylene blue and methyl orange from aqueous solution by iron oxide-coated zeolite in fixed bed column: predicted curves. Desalin Water Treat 22(1–3):258–264